

Experimentally validated numerical method for the hydrodynamic design of horizontal axis tidal turbines

W.M.J. Batten^{a,*}, A.S. Bahaj^a, A.F. Molland^b, J.R. Chaplin^a,
Sustainable Energy Research Group

^a*School of Civil Engineering and the Environment, University of Southampton, UK*

^b*School of Engineering Sciences, Ship Science, University of Southampton, UK*

Received 26 March 2006; accepted 21 April 2006

Available online 10 October 2006

Abstract

Although a lot can be learnt from technology transfer from wind turbines and ship propellers, there have been a few experiments investigating marine current turbines. As a result, a study has been carried out on the power, thrust and cavitation characteristics of 1/20th scale model of a possible 16 m diameter horizontal axis tidal turbine. Cavitation tunnel experiments for different blade pitch settings have been compared with simulations based on a developed blade element-momentum theory. This theory has been shown to provide a satisfactory representation of the experimental turbine performance characteristics. As an example application, the developed theory has been used to design possible horizontal axis tidal turbines for the tidal flows around Portland Bill. The results show that there is a clear balance between design loads and optimisation of energy yields.

© 2006 Elsevier Ltd. All rights reserved.

Keywords: Tidal energy; Marine current energy; Tidal turbine

1. Introduction

There is a growing market for ‘green’ electrical energy derived from sustainable resources throughout the world. Many countries are offering government sponsored incentives and targets, such as the UK with 10% by 2010 and 20% by 2020 from renewable sources. The oceans around the world offer a large energy source that is yet to be significantly tapped. Although the power from waves and ocean thermal currents are larger, tidal or marine currents with peak flows of over 4 kn (~ 2 m/s), caused by constrained topography, offer an exciting proposition for the extraction of predictable energy. Many devices are being studied for marine current energy conversion although most are designed around underwater wind turbine, known as a marine current turbine (MCT) (Fraenkel, 2002).

There have been a few published studies concerning the exploitation of tidal marine currents around UK waters such as DG Science (1996) and Binnie Black & Veatch Ltd (2001); these suggest that energy production of 10–30 TWh/year is possible. Based on the UK electrical consumption of 401 TWh/year for 2003 (Digest of UK Energy Statistics, 2004), MCTs could supply 2.5–7.5% of the current UK energy demand. One such site is the Race of Alderney in the Channel Islands, which could supply 1.34 TWh/year with large farm of MCTs (Bahaj and Myers, 2004; Myers and Bahaj, 2005). The ability to exploit such a site is dependent on predicting their hydrodynamic characteristics for which methodologies need be established that describe the physical and operational performance of the turbines, allowing designs to be investigated and performance evaluated.

To an extent, much can be transferred from the design and operation of wind turbines (Burton et al., 2000) and ship propellers (Carlton, 1994). There are, however, a number of fundamental differences in the design and operation of MCTs which will require further investigation, research and development. These include changes in

*Corresponding author. Tel.: +44 23 8059 2051;
fax: +44 238 8067 8606.

E-mail address: wmjb@soton.ac.uk (W.M.J. Batten).

URL: <http://www.energy.soton.ac.uk>.

Nomenclature

A	rotor area (m^2)
c	chord (m)
C_L	lift coefficient
C_D	drag coefficient
C_P	power coefficient
C_T	thrust coefficient
P	rotor power (Watts)
Q	rotor torque (Nm)

r	local radius (m)
R	rotor radius (m)
t	section thickness (m)
T	rotor thrust (N)
TSR	tip speed ratio = $\Omega R/U_0$
U_0	free stream speed (m/s)
α	section incidence (deg)
ρ	density of water (kg/m^3)
Ω	rotational speed of rotor (rad/s)

force loadings, depth of immersion and the possible occurrence of cavitation.

The experimental results from cavitation tunnel tests, discussed and used for validation of the numerical method within this paper are from a scope of a much larger set of tests. These tests were carried out in both cavitation tunnel and towing tank; they included the cavitation inception observations, effect of yaw, tip emersion and dual rotor interactions. These experimental results are discussed in full in Bahaj et al. (2007) and full details of the experimental rig design along with tabulated data from the tests are presented in Bahaj et al. (2005).

2. Experimental procedure

2.1. Test facilities

Measurements of the torque and thrust characteristics of an 800 mm rotor were carried out in a cavitation tunnel at QinetiQ, Haslar. The experimental rig in the cavitation tunnel is shown in Figs. 1 and 2. The tunnel has a working section of 2.4×1.2 m and a maximum flow speed of 8 m/s. This provided a controlled environment for the principal

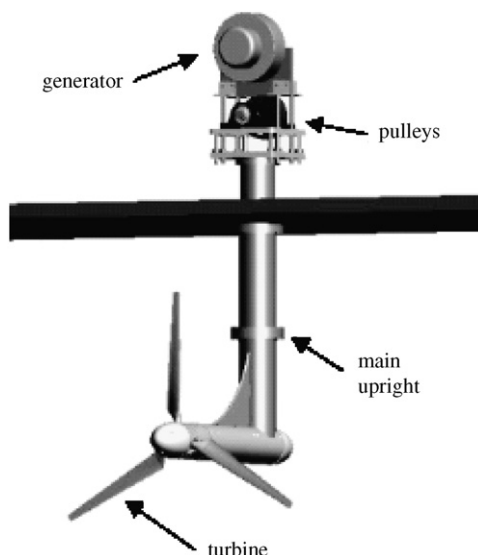


Fig. 1. Visualisation of the experimental rig in the cavitation tunnel.

measurements with zero yaw and cavitation inception observations.

2.2. Models

A rotor diameter of 800 mm was chosen as a compromise between maximising Reynolds number and not incurring excessive tunnel blockage correction. The boss diameter to suit the test rig was 100 mm. The blades were developed from the profile shape of a NACA 63-8xx and with a chord, thickness and pitch distribution presented in Table 1. The model blades were milled on a 5-axis CNC machine from aluminium alloy in the University workshops. The rotor hub has two halves that clamp the blades, allowing changes in pitch to be made. The hub pitch is defined at 20% radius where the section was interpolated to a circle at the hub.

2.3. Test rig

In order to test model rotors an experimental test rig that could be bolted to either the carriage of the towing tank or the ceiling of the cavitation tunnel was designed. Construction was carried out in the University workshops. The rig is currently designed to accommodate model rotors up to about 900 mm in diameter. The rotor is attached to a



Fig. 2. Photograph of the assembled test rig in the cavitation tunnel.

Table 1
Particulars of turbine blades and hub

r/R	r (mm)	c/R	Pitch (deg.)	t/c (%)
0.2	80	0.1250	20.0	24.0
0.3	120	0.1156	14.5	20.7
0.4	160	0.1063	11.1	18.7
0.5	200	0.0969	8.9	17.6
0.6	240	0.0875	7.4	16.6
0.7	280	0.0781	6.5	15.6
0.8	320	0.0688	5.9	14.6
0.9	360	0.0594	5.4	13.6
1.0	400	0.0500	5.0	12.6

main shaft which drives a DC generator from a pulley through a belt carried up through the vertical support tube (Fig. 1). A photograph of the test rig set-up in the cavitation tunnel is shown in Fig. 2.

An in-line strain gauge dynamometer mounted next to the turbine was used to measure the thrust and torque. This dynamometer was designed to run wet, so measurements could be made before any bearing or seal losses. The strain gauge bridge circuit is connected via a slip-ring assembly to conditioners and output signals were acquired on a computer. The electrical power is absorbed with rheostats, which also allowed regulation of the rotor speed. Full details of the experiment test rig, models and results are given in Bahaj et al. (2007).

3. Data reduction

3.1. General

For a given tunnel flow speed and rotational speed the torque and the thrust were acquired from the dynamometer. The averaged excitation voltages from the torque and thrust bridge circuits were corrected for zero offset and then multiplied by the calibration factor to resolve the torque (Q) and thrust (T). The power (C_P) and thrust (C_T) coefficients were defined in the following way:

$$\text{Power coefficient } C_P = \frac{Q\Omega R}{(1/2)\rho U_T^3 A}, \quad (1)$$

$$\text{Thrust coefficient } C_T = \frac{T}{(1/2)\rho U_T^2 A}, \quad (2)$$

where A is the rotor area, and U_T is the tunnel speed.

3.2. Blockage correction

The normal boundary corrections for propellers are not suitable for negative thrust (effectively the case of a generating turbine). In order to correct for blockage, Glauert's (1947) equations have been modified for wake expansion in the case of a turbine by Barnsley and Wellicome (1990). The equations are presented in Bahaj et al. (2005) and are used to correct for boundary layer

effects to present results based on free stream inflow speed (U_0). For example, with a thrust coefficient of 0.8, the corrections amounted up to 18% decrease in power coefficient and 11% decrease in thrust coefficient.

4. Numerical method

Blade element-momentum (BEM) theory is used, which is based on a combination of momentum theory and blade element theory. The momentum theory is used to derive the axial and circumferential inflow factors, with the introduction of a tip loss factor to take into account the finite number of rotor blades. The blade element theory is used to model the section drag and torque by dividing the rotor blade into a number of elemental sections. The integration of these values across the blade allows the derivation of thrust and power coefficients for the rotor.

The adapted numerical program is based on BEM theory and the program for wind turbine design developed by Barnsley and Wellicome (1990). However, the code developed has major enhancements specifically established to deal with the operation in water and other additions including the pressure increase due to wake (Burton et al., 2000), new extrapolation for stall data (Snel et al., 1994). Further details are in Batten et al. (2006).

For the lift and drag coefficient data required to solve for the blade elements, the 2D panel code Xfoil (Drela and Giles, 1987) was used. Xfoil is a linear vorticity stream function panel method which includes a viscous solution which interacts with the incompressible potential flow via a surface transpiration model. Recent cavitation tunnel tests for NACA sections suitable towards the tip of a MCT have been compared with Xfoil (Molland et al., 2004). The results showed good agreement with pressure distributions and lift curves but underestimate drag coefficients at incidences approaching stall angle.

The developed theory has been used to solve for the model turbine tested in the cavitation tunnel. The chord, pitch and thickness distributions in Table 1 have been used to define the blade shape. The basic section lift and drag data are shown in Fig. 3 for three thickness ratios solved using Xfoil. To extrapolate up to the stall delay angle the method proposed by Snel et al. (1994) was used. Further extrapolations beyond the stall delay angle were achieved using Viterna and Corrigan (1981) methodology for post-stall predictions. Fig. 4 shows the interpolated and extrapolated lift and drag data from -10° to 60° for four radial positions. This figure shows the strong influence of the stall delay equations used towards the hub. This data set along with the blade shape data is used as the input data for the developed BEM theory.

5. Comparison between experiment and theory

The BEM theory has been validated using the cavitation tunnel tests for the 800 mm diameter turbine; the case for 20° - and 25° -hub pitch is shown in Figs. 5 and 6. The power

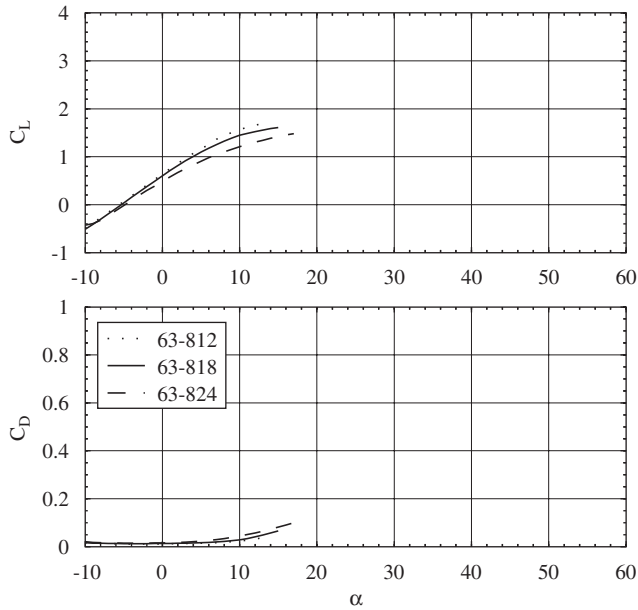


Fig. 3. 2D lift and drag section data solved using XFOil.

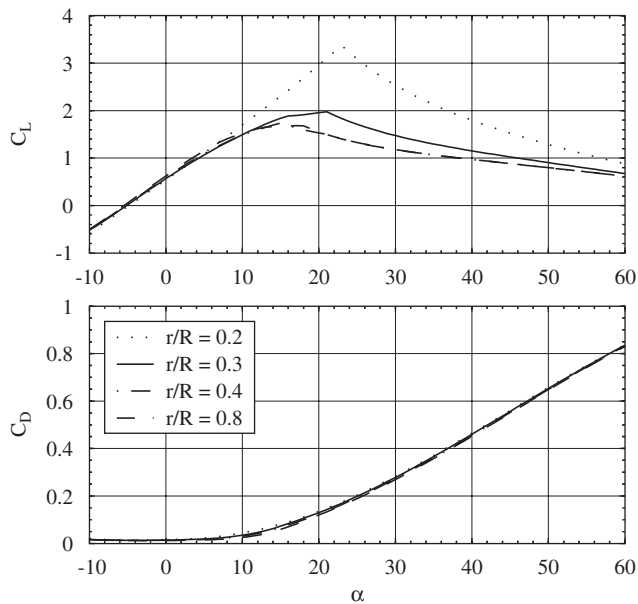


Fig. 4. 2D lift and drag characteristics interpolated and extrapolated with stall delay.

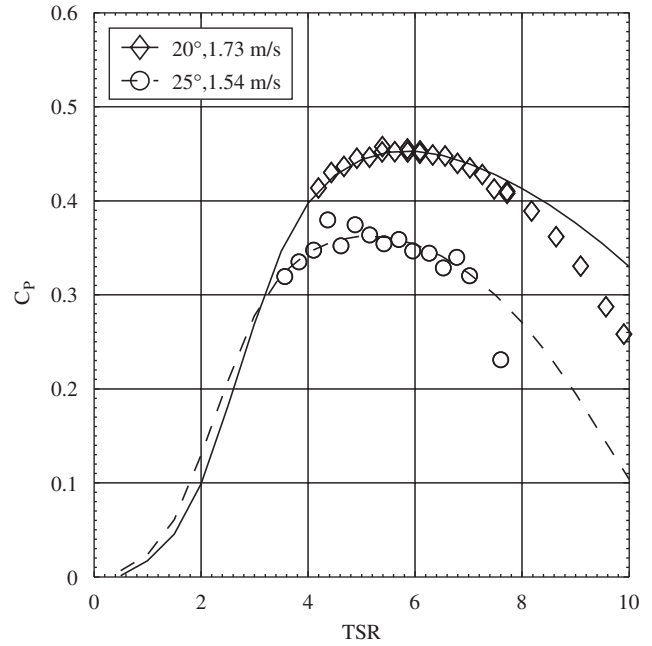


Fig. 5. Cavitation tunnel power coefficient (C_P) measurements versus theoretical results.

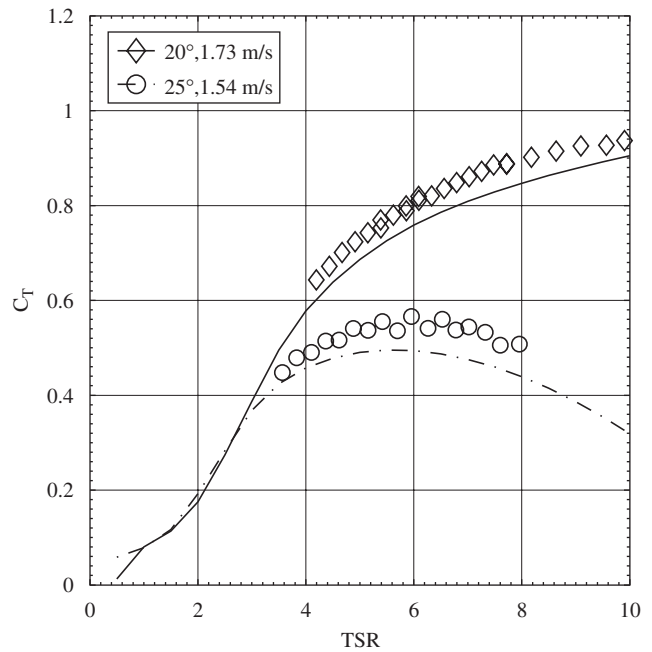


Fig. 6. Cavitation tunnel thrust coefficient (C_T) measurements versus theoretical results.

coefficient measurements, Fig. 5, show good agreement for $TSR = 3-7$, within the experimental scatter. While with $TSR > 7$ the theory tended to over predict. Fig. 6 shows constant experimental data with the numerical simulations under predicting by around 5–10% for the 20°-hub pitch case and 5–15% for the 25°-hub pitch.

Many experimental tests were carried out for a wide range of hub pitch angles in both cavitation tunnels and towing tanks. The accuracy of the predictions, as can be seen from the typical results shown in Figs. 5 and 6 is more than satisfactory for using the developed theoretical tools for design exercises and parametric studies.

6. Matching turbine design to the tidal velocity data

6.1. General

For the example turbine design the following was assumed:

- the turbine had 16 m diameter;
- the blade shape was that of the experiment with a hub pitch of 20° at the design speed;

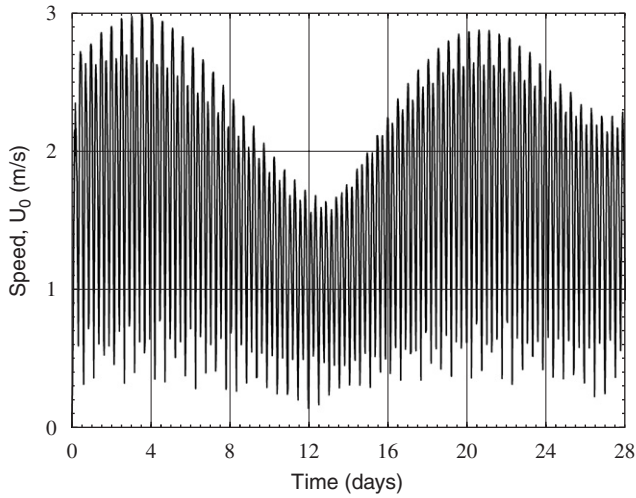


Fig. 7. Simulated tidal velocity data for a site near Portland Bill over a Lunar month.

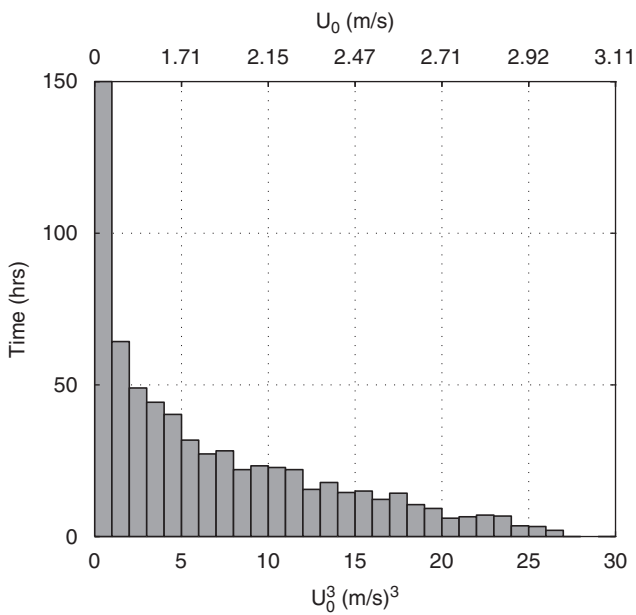


Fig. 8. Histogram of the cubed tidal velocity data for Portland Bill over a Lunar month.

- the gear box and seals were of a constant 97% efficiency;
- the generator was constant rpm with an constant efficiency of 95%;
- above the design speed the turbine blades were pitched to maintain a constant power;
- the turbine was yawed towards the tidal flow;
- the cut speed for operation is determined from the power required to overcome the generator and gear box efficiencies at the rated power of the device.

Tidal velocity data presented in Fig. 7, and derived by Blunden and Bahaj (2004) from simulations near Portland Bill have been used here to illustrate the applicability of the developed tools. The tidal velocity data is mean depth averaged, at 15 min intervals, for one Lunar month mid way between spring and neap tides. From this data set it is possible to present the data in a histogram of hours at a given speed cubed as shown in Fig. 8.

The speeds (U_0) are distributed as cubes to give more accurate predictions as power is proportional to the cube of the speed. Based on preliminary simulations of energy yield, the use of cubic distribution reduced the number of bins in the histogram by over 3 when compared with time stepping over the whole month of velocity data. This tidal energy histogram is clearly very different from wind velocity data at wind farms with distribution such as the Weibull (Burton et al., 2000) with zero hours with near zero m/s.

6.2. Matching design speed to the tidal data

From the assumed turbine design, the power coefficient curve (Fig. 5) and the velocity histogram (Fig. 8), the suitable design TSR and design speed are unclear, although the following might be expected ($4 < \text{TSR} < 7$) and ($2 < U_{\text{Des}} < 3$).

Applying the assumed turbine design and the developed BEM theory the energy over the Lunar month has been calculated from the histogram of tidal velocity data. Table 2 shows the results for a range of TSR and design speeds. The general trend shows that as design speed increases from 2 to 3 m/s a slowing in the increase in energy but large increases in maximum thrust occur. The results in

Table 2
Possible configurations over the Lunar month at Portland Bill

Design TSR	Design speed (m/s)	Rated power (kW)	Maximum thrust (kN)	Energy yield (MWh)	Load factor
4	2.00	287	238	111	0.69
4	2.25	409	301	137	0.67
4	2.50	560	372	157	0.41
4	2.75	746	450	170	0.34
4	3.00	969	535	173	0.27
5	2.00	325	283	121	0.55
5	2.25	464	358	146	0.47
5	2.50	636	442	164	0.38
5	2.75	846	535	171	0.30
5	3.00	1098	637	168	0.23

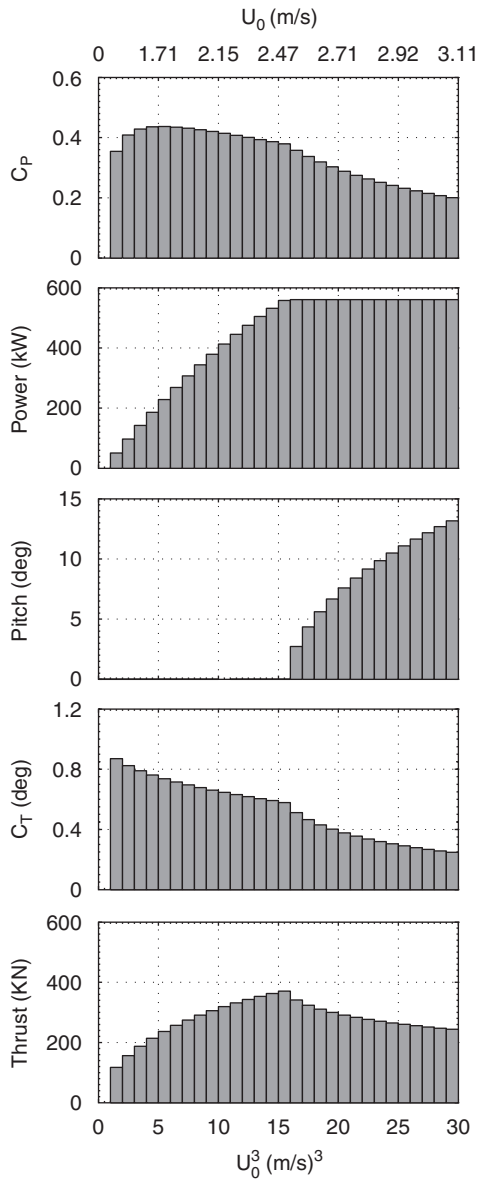


Fig. 9. Turbine at a design speed of 2.5 m/s, rated power 636 kW, 16 m diameter and a design TSR = 4.

Table 2 show that a jump in design TSR from 4 to 5 resulted in over 10% increase in maximum thrust. Such results, as will be discussed later, will have a profound impact on MCT design philosophy and installation costs.

Example results for a design speed of 2.5 m/s and TSR of 4 and 5 are shown, respectively, in Figs. 9 and 10. Although the rated power is over 10% higher for the design TSR of 5 the power produced is only 5% higher whilst the maximum thrust experienced is 15% higher. The choice of a low TSR has two effects, firstly, the design C_p is lower this means that although there is not as high a rated power at slow tidal speeds (high TSR) the turbine will be more efficient and consequently produce similar amounts of energy. Secondly, the lower TSR corresponds to a lower C_T on the graph therefore the lower the maximum thrust. From this analysis there is clearly a balance between the costs of

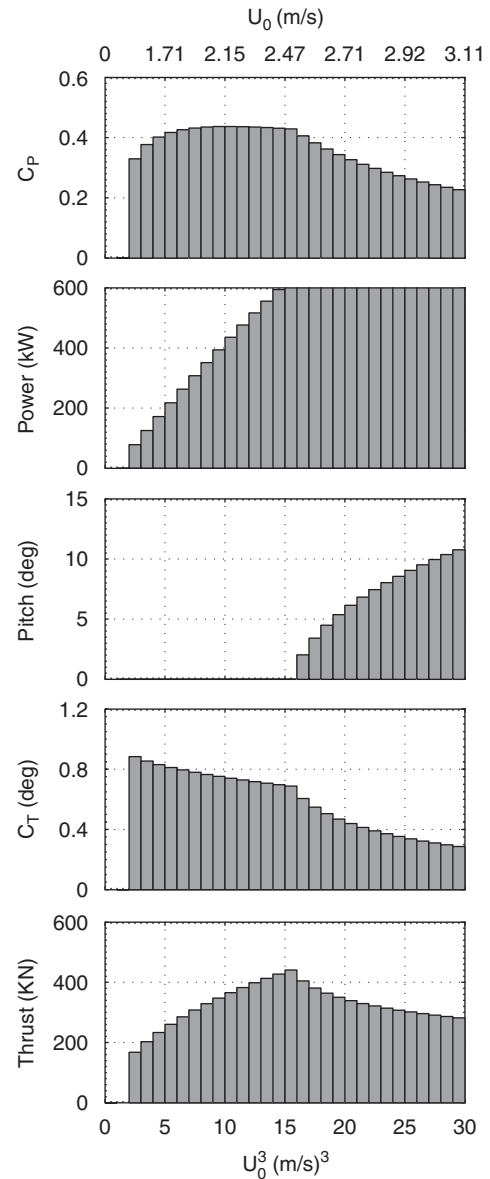


Fig. 10. Turbine at a design speed of 2.5 m/s, rated power 636 kW, 16 m diameter and a design TSR = 5.

designing turbine and support structures for the extra loads and rated power with small increases in annual energy output.

Fig. 11 shows the energy output over the Lunar month for four design speeds, the lower speed showing an almost linear increase in energy, while the high design speeds show a lag in energy output during the spring tides. Consequently a lower design speed with a high load factor of over 0.5 may produce a better base supply load to the grid.

6.3. Optimisation of design speeds

In order to search for optimum design TSR and operation speed for maximum energy over the Lunar month for a given thrust, the Nelder–Mead nonlinear regression algorithm (MathWorks, 2001) was applied. The

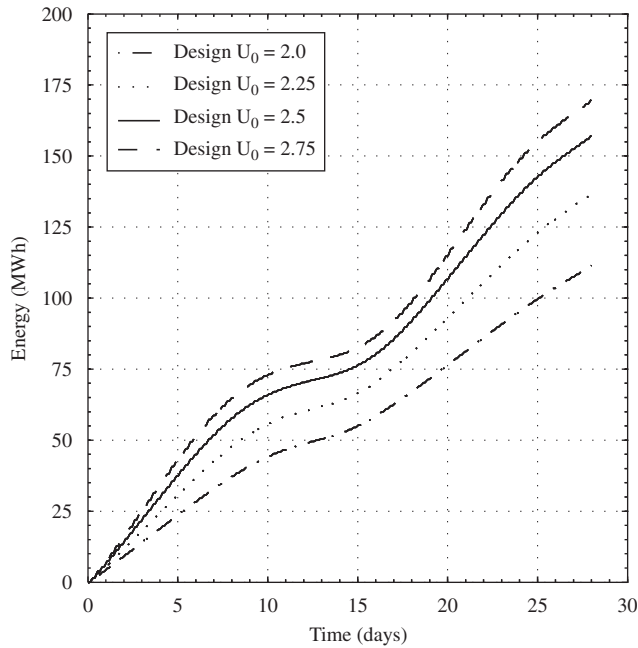


Fig. 11. Comparison of the energy output from a 16m turbine at a TSR of 4.

Table 3
Optimised configurations over the Lunar month at Portland Bill

Maximum thrust (kN)	Design TSR	Design speed (m/s)	Rated power (kW)	Energy (MWh)	Load factor
200	3.16	2.16	256	100	0.58
300	3.44	2.48	451	140	0.46
400	3.90	2.61	626	162	0.38
500	4.21	2.83	848	173	0.30
551	4.31	2.94	966	174	0.26

results from this study are presented in Table 3. When the thrust is not limited the maximum peak energy output of 174 MWh and also the maximum thrust of 551 kN are achieved. These results show a similar slowing in increase in energy with increased loadings as shown in Fig. 12. For example, the case limiting the thrust to 300 kN produces energy of 140 MWh, which is only 20% less than the maximum achievable, while the reduction in thrust load is 55%. This clearly shows that there is a balance that needs to be addressed between the energy yield over the lifetime and installation costs for high load devices.

7. Conclusion

The test programmes carried out at Southampton University on model MCT and the developed blade element theory have shown good agreement with experiments. In essence, the wide-ranging results satisfactorily validated the developed blade element theory. This

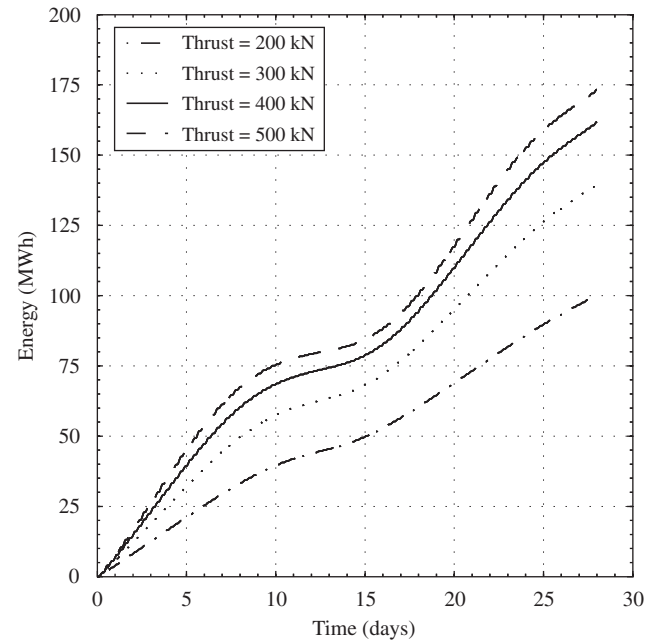


Fig. 12. Comparison of the energy output from a 16 m turbine for a range of limiting thrust.

numerical method can now be used as a tool for designing and optimising energy output with tidal data.

For the example case of matching the turbine design to the tidal flow data around Portland bill there is clearly a balance between the maximum design loads and the energy output from the turbine. Also demonstrated is the possible high load factors that could supply a better load to the grid.

An optimisation program is demonstrated to provide a method of matching design speeds for a given design of support structure. As the optimum energy output is approached for a particular turbine design there can be substantial increases in loads with small increases in annual energy output.

The work presented here linking device and site parameters represents the initial analysis of optimising energy yields whilst keeping an idea on the other issue like maximum stress and its impact on device costs. Further work is currently being conducted to identify the balance between energy yield and system cost for various marine current sites around the UK.

Acknowledgement

The work described in this paper covers part of a research project funded by the Engineering and Physical Science Research Council. Grant GR/R50424/01.

References

- Bahaj, A.S., Myers, L.E., 2004. Analytical estimates of the energy yield potential from the Alderney Race (Channel Islands) using MCTs. *Renewable Energy* 29 (12), 1931–1945.

- Bahaj, A.S., Chaplin, J.R., Molland, A.F., Batten, W.M.J., 2005. Experimental investigation into the hydrodynamic performance of marine current turbines. Sustainable Energy Series, Report No. 3, Southampton University.
- Bahaj, A.S., Molland, A.F., Chaplin, J.R., Batten, W.M.J., 2007. Power and thrust measurements of marine current turbines under various hydrodynamic flow conditions in a cavitation tunnel and a towing tank. *Renewable Energy* 32 (3), 407–426.
- Barnsley, M.J., Wellicome, J.F., 1990. Final report on the 2nd phase of development and testing of a horizontal axis wind turbine test rig for the investigation of stall regulation aerodynamics. Carried out under ETSU Agreement E.5A/CON5103/1746.
- Batten, W.M.J., Bahaj, A.S., Molland, A.F., Chaplin, J.R., 2006. The prediction of the hydrodynamic performance of marine current turbines. *Renewable Energy*, in review.
- Binnie Black & Veatch Ltd, 2001. Commercial prospects for tidal stream power. Redhill, DTI/ETSU, Harwell.
- Blunden, L., Bahaj, A.S., 2004. Initial evaluation of tidal stream energy resources at Portland Bill, UK. World Renewable Energy Conference VIII. Elsevier, Denver, Colorado, USA.
- Burton, T., Sharpe, D., Jenkins, N., Bossanyi, E., 2000. *Wind Energy Handbook*. Wiley.
- Carlton, J.S., 1994. *Marine Propellers and Propulsion*. Butterworth-Heinemann.
- DG Science, 1996. The exploitation of tidal marine currents (non-nuclear energy JOULE II project results). Report EUR 16683, Research and Development, European Commission Office for Official Publications, The European Commission, Luxembourg.
- Digest of UK Energy Statistics, 2004. Available from the Internet, http://www.dti.gov.uk/energy/inform/energy_stats/.
- Drela, M., Giles, M.B., 1987. Viscous-inviscid analysis of transonic and low Reynolds number airfoils. *AIAA Journal* 25 (10), 1347–1355.
- Fraenkel, P.L., 2002. Power from marine turbines. *Proceedings of the Institution of Mechanical Engineers Part A* 216, 1–14.
- Glauert, H., 1947. *The Elements of Aerofoil and Airscrew Theory*, second ed. Cambridge University Press.
- MathWorks, 2001. MATLAB [CDROM], ver 6 rel 5, [Computer programme]. Available from the Internet, <http://www.mathworks.com>.
- Molland, A.F., Bahaj, A.S., Chaplin, J.R., Batten, W.M.J., 2004. Measurements and predictions of forces, pressures and cavitation on 2-D sections suitable for marine current turbines. *Proceedings of the Institution of Mechanical Engineers Part M* 218, 127–138.
- Myers, L.E., Bahaj, A.S., 2005. Simulated electrical power potential harnessed by marine current turbine arrays in the Alderney Race. *Renewable Energy* 30 (11), 1713–1731.
- Snel, H., Houwink, R., Bosschers, 1994. Sectional prediction of lift coefficients on rotating wind turbine blades in stall. Report ECN-C—93-052, Energy Research Centre of the Netherlands.
- Viterna, L.A., and Corrigan, R.D., 1981. Fixed pitch rotor performance of large horizontal axis wind turbines, DOE/NASA Workshop on Large Horizontal Axis Wind Turbines, Cleveland, Ohio.